ARTICLE

Turbulent Transport of Momentum and Scalars Above an Urban Canopy

Linlin Wang · Dan Li · Zhiqiu Gao · Ting Sun · Xiaofeng Guo · Elie Bou-Zeid

Abstract Turbulent transport of momentum and scalars over an urban canopy is investigated using the quadrant analysis technique. High-frequency measurements are available at three levels above the urban canopy (47, 140 and 280 m). The characteristics of coherent ejection–sweep motions (flux contributions and time fractions) at the three levels are analyzed, particularly focusing on the difference between ejections and sweeps, the dissimilarity between momentum and scalars, and the dissimilarity between the different scalars (i.e., temperature, water vapour and CO_2). It is found that ejections dominate momentum and scalar transfer at all three levels under unstable conditions, while sweeps are the dominant eddy motions for transporting momentum and scalars in the urban roughness sublayer under neutral and stable conditions. The flux contributions and time fractions of ejections and sweeps can be adequately captured by assuming a Gaussian joint probability density function for flow variables. However, the inequality of flux contributions from ejections and sweeps is more accurately reproduced by the third-order cumulant expansion method (CEM). The incomplete cumulant expansion method (ICEM) also works well except for CO_2 at 47 m where the skewness of CO_2 fluctuations is significantly larger than that for vertical velocity. The dissimilarity between momentum and scalar transfers is linked to the dissimilarity in the characteristics of ejection–sweep motions and is further quantified by measures of transport efficiencies. Atmospheric stability is the controlling factor for the transport efficiencies of momentum and heat, and fitted functions from the literature describe their behaviour fairly accurately. However, transport efficiencies of water vapour and CO_2 are less affected by the

L. Wang · Z. Gao · X. Guo
State Key Laboratory of Atmospheric Boundary Layer Physics and Atmospheric Chemistry,
Institute of Atmospheric Physics, Chinese Academy of Sciences, Beijing, China

D. Li (✉) · E. Bou-Zeid
Department of Civil and Environmental Engineering, Princeton University,
Princeton, NJ 08540, USA
e-mail: danl.princeton.2009@gmail.com

T. Sun
State Key Laboratory of Hydroscience and Engineering, Department of Hydraulic Engineering,
Tsinghua University, Beijing, China

atmospheric stability. The dissimilarity among the three scalars examined in this study is linked to the active role of temperature and to the surface heterogeneity effect.

Keywords Ejections and sweeps · Quadrant analysis · Reynolds analogy · Scalar similarity · Transport efficiency · Urban canopy

1 Introduction

A better understanding of the transport of momentum and scalars (heat, water vapour, carbon dioxide, etc.) at the air-surface interface and in the turbulent atmospheric boundary layer (ABL) is of crucial importance for the parametrizations of land–atmosphere exchanges in numerical weather prediction models. It can also have positive impacts in a range of disciplines such as hydrology and ecology. Coherent turbulent motions have been shown to be responsible for a large fraction of these momentum and scalar fluxes (Robinson 1991; Marusic et al. 2010; Smits et al. 2011). Their characteristics have been studied over different natural surfaces, including water (Li and Bou-Zeid 2011), vineyards (Francone et al. 2012), and vegetation canopies (see e.g., Shaw et al. 1983; Paw et al. 1992; Katul and Cl 1997; Katul et al. 1997; Poggi et al. 2004; Dupont and Patton 2012; see Raupach and Thom 1981 and Finnigan 2000 for comprehensive reviews). Many studies have also examined coherent structures and their influence on turbulent flow and transport over urban canopies (e.g., Rotach 1993a,b; Roth 1993; Roth and Oke 1993, 1995; Grimmond and Oke 2002; Kanda et al. 2004; Feigenwinter and Vogt 2005; Kanda 2006; Moriwaki and Kanda 2006; Christen et al. 2007, 2009; Horiguchi et al. 2010; lnagaki and Kanda 2010; Wood et al. 2010; also see Roth 2000 and Fernando 2010 for comprehensive reviews). While these studies have considerably advanced our understanding of urban flow and turbulence, many open questions remain particularly in relation to the characteristics of coherent structures in urban environments, how they are modulated by atmospheric stability, and how they affect urban-atmosphere exchanges of momentum and scalars. In addition, urban morphology, which significantly affects urban flow and turbulence (see e.g., Wood et al. 2010), as well as the urban surface energy balance (see e.g., Piringer et al. 2002; Grimmond et al. 2010, 2011) and hence stability, varies significantly between different cities. Additional analyses are therefore needed to generalize the effect of urbanization on coherent turbulent motions and on momentum and scalar transport over urban canopies. Such conclusions can help improve high-resolution urban microclimate models (see e.g., Chen et al. 2011; Wang et al. 2013) and air quality models in urban terrain (see e.g., Britter and Hanna 2003; Fernando et al. 2010), which are becoming increasingly indispensable considering the sustained and rapid growth of the urban population (Grimm et al. 2008).

Due to aerodynamic and thermodynamic differences between bluff buildings and permeable plants, turbulent flow over urban canopies shows distinct features as compared to that over vegetation canopies (see Roth 2000 for a review). For example, the form drag due to bluff buildings augments the turbulent transport of momentum in urban canopies but has no effect on the transport of scalars; on the other hand, the leaves and trunks in vegetation canopies offer more exchange surfaces for scalars as compared to buildings but resist the flow less than bluff bodies. As such, turbulent structures and turbulent transports of momentum and scalars are expected to be different over an urban canopy compared to their counterparts over a vegetation canopy. Despite these distinctions, the subdivision of the ABL into various layers has conventionally followed similar criteria and nomenclatures over the two types of canopies. The flow over urban areas in the atmospheric boundary layer (i.e., the urban
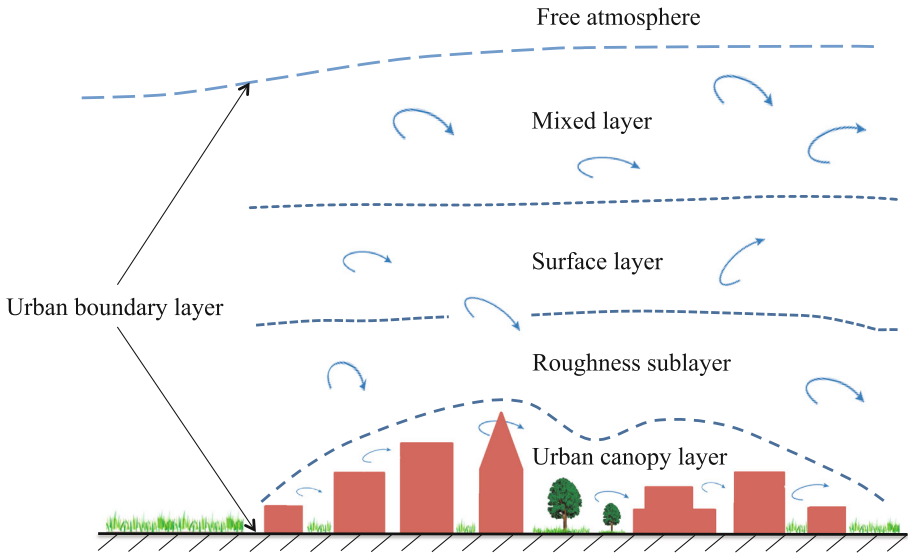
Fig. 1 Different sublayers of an urban boundary layer (following the classification of Oke 1988)

boundary layer) can conceptually be subdivided into different regimes: the urban canopy, the roughness sublayer, the surface layer and the outer (mixed) layer (see Fig. 1). The urban canopy layer usually refers to the layer from the ground to the rooftop level; in that layer the flow is very complex and mainly determined by the geometry of the canopy in the vicinity of the point of interest. The roughness sublayer is the layer in which the atmospheric flow is still affected by individual roughness elements but where turbulence has initiated its homogenization of the flow. The roughness sublayer is typically of thickness $2 \sim 5H_b$, where H_b is the average building height (Roth 2000; Arnfield 2003; Fernando 2010). Above the roughness sublayer, turbulent mixing has completely blended the effects of individual roughness elements, creating a layer in which the wind profile is logarithmic under neutral conditions and turbulent fuxes are nearly constant with height. This is the surface layer as shown in Fig. 1, which is also sometimes referred to as the constant-flux layer (see e.g., Arnfield 2003; Fernando 2010). Above the surface layer is the outer layer where the wind profile is no longer logarithmic and the fluxes vary significantly with height. It is also called the mixed layer under unstable conditions in which the profiles of mean wind and scalar concentrations are almost constant. Except for some wind-tunnel and large-eddy simulation studies (see e.g., Kanda et al. 2004; Kanda 2006; Inagaki and Kanda 2010; Böhm et al. 2012), there has been no consistent study on the characteristics of coherent eddy structures in various sublayers over real urban terrain (i.e., the roughness sublayer, the surface layer, and the outer layer). This is related to the scarcity of very tall meteorological towers that span several of these sublayers in densely built areas.

In this study, we explore the characteristics of turbulent structures over a real, highly-urbanized surface in a major city (Beijing, China) with turbulence measurements from a very tall tower at three different levels: 47, 140, and 280 m. It has been shown that measurements at 47 m are within the roughness sublayer (Miao et al. 2012), given that the characteristic building height for that area is $18 \sim 19$ m (Miao et al. 2012) and that there are very tall buildings ($70 \sim 90$ m) within a circle of about 1-km radius (AI-Jiboori 2008). Measurements at 140 m should be above the roughness sublayer when the height of the roughness sublayer

is estimated based on the mean building height, but some effects from the very tall buildings might be noticeable; these measurements are within the surface layer (Miao et al. 2012). Measurements at 280 m are typically in the outer layer.

Another prominent feature of urban terrain is the significant spatial heterogeneity in the source/sink distributions of momentum and different scalars, which will reinforce the effects of thermal stability to influence the similarity, or lack thereof, of turbulent transports. Previous studies have shown that atmospheric stability is a critical factor that controls momentum–scalar transport dissimilarity (Li and Bou-Zeid 2011; Dupont and Patton 2012), while the transport similarity between different scalars is primarily affected by surface source/sink distributions (Moriwaki and Kanda 2006; Williams et al. 2007; Detto et al. 2008; Moene and Schuttemeyer 2008; Iwata et al. 2010) and non-local effects such as advection and entrainment (Bruin et al. 1999; Sempreviva and Gryning 2000; Lee et al. 2004; Asanuma et al. 2007; Cava et al. 2008; Katul et al. 2008; Li et al. 2012). Nevertheless, most of these studies focus on the dissimilarity between temperature and water vapour (see e.g., Cava et al. 2008; Detto et al. 2008; Katul et al. 2008; Moene and Schuttemeyer 2008; Li et al. 2012; Zhao et al. 2013). Less is known about the dissimilarity between temperature and CO_2, and the dissimilarity between water vapour and CO_2, particularly in urban environments. A notable exception is the study by Moriwaki and Kanda (2006), which examined the dissimilarity among temperature, water vapour and CO_2 over a suburban area of Tokyo, Japan but only under unstable conditions. Their results indicate that heat is always transferred by thermal and organized motions more efficiently than water vapour and CO_2. The dissimilarity is also caused by the heterogeneity in the source distributions of these scalars since, if the surface sources are well correlated for sensible heat, water vapour, and CO_2, the two passive scalars would accompany temperature in these thermals and the dissimilarity would not be detectable. These observations were later confirmed by Nordbo et al. (2013) using datasets collected at three locations in Helsinki. Moreover, Nordbo et al. (2013) reported that the transport of sensible heat is less efficient than transports of water vapour and CO_2 under stable conditions. They also observed significant intra-city variability in turbulent transport efficiencies of scalars, suggesting that some determining physical factors that vary between these locations remain elusive. This motivates us to investigate the dissimilarity in turbulent transports of momentum and scalars as well as the dissimilarity among turbulent transports of different scalars using the Beijing tower datasets under both unstable and stable conditions.

The paper is organized in the following way: Sect. 2 describes the dataset and methodology and Sect. 3 presents the main results and discussions. Conclusions are presented in Sect. 4.

2 Data and Methodology

2.1 Experimental Set-Up and Data Processing

The data used in the study were obtained at an urban site in Beijing, China (39.97°N, 116.37°E) between May 1 and August 31 2011. The flux tower is 325 m high and has turbulence measurements at three different levels: 47, 140 and 280 m. The location of the tower and the impervious surface fraction in the surrounding areas are shown in Fig. 2. Since no simple analytical footprint model exists for heterogeneous surfaces, and since the impact of stability on such footprints is complex and poorly understood, we make a simple estimate of the footprint of the measurement at different heights to serve a guideline of the sampled area. This simple estimate suffices since the details of the footprint are not quantitatively
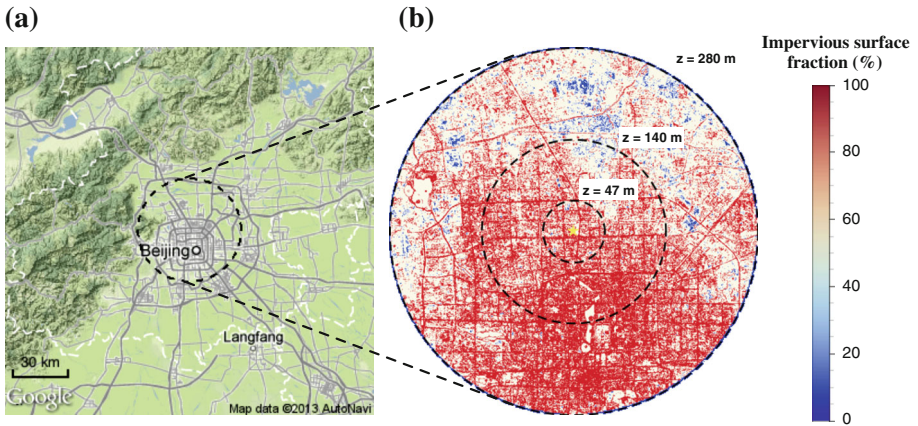
Fig. 2 a Topographic map of Beijing (courtesy of Google). **b** The impervious surface fraction retrieved from Landsat TM5 satellite image on 28 May, 2007. The *circles* roughly indicate the footprints of measurements at different heights and have radii of 100z where z is the sensor height. The *yellow star* in **b** denotes the position of the Beijing Tower (39.97°N, 116.37°E)

Table 1 Fractions of land-cover types within the footprints of measurements at three levels on the Beijing Tower

Height (m)	Impervious	Vegetated	Soil
47	0.74	0.05	0.21
140	0.73	0.05	0.22
280	0.67	0.05	0.28

used in any of our analyses. Noting that the internal boundary and equilibrium layer heights under neutral conditions grow roughly as $(1/10)x$ and $(1/100)x$ respectively (x is the fetch after some surface transition, see e.g., Brutsaert 1982), but that under unstable conditions the internal boundary layer can grow much faster than $(1/10)x$, we estimate the footprint of a measurement at height z as a circle of radius 100z that is centred at the flux tower. These circles are shown in Fig. 2 and will simply be referred to as "footprints" hereafter. Hence, we are not explicitly tracking the exact source areas of turbulent fluxes and the details of each transition from one land cover to another; we are rather interested in a qualitative assessment of surface heterogeneity.

The surface compositions in the footprints of the flux tower are separated into three categories: impervious (including both ground and buildings), vegetated, and bare soil; the categorization is obtained by processing the Landsat TM5 images (of horizontal resolution 30 m). The details for the processing procedures follow Wu and Murray (2003) and Hou et al. (2013). As can be seen from Fig. 2 and Table 1, impervious/built-up surfaces are the dominant land-cover type. The fractions of impervious surfaces in all of the three footprints exceed 65 %; but they decrease from the innermost footprint, corresponding to the lowest measurement level, to the outermost footprint, corresponding to the highest measurement level. Bare soil is the second most common surface type with fractions ranging from 20 to 30 %, while vegetated surfaces have the lowest fractions and the fractions in the three footprints are 5 %.

The measurements available at this flux tower have been reported elsewhere (AI-Jiboori et al. 2002; AI-Jiboori 2008; Li et al. 2010; Miao et al. 2012), along with other site and experimental details. Therefore, only instruments, data and methods of specific relevance to this

study are described here. As mentioned earlier, the flux tower is 325 m high and has turbulence measurements at 47, 140 and 280 m. Three-dimensional sonic anemometers (CSAT3, Campbell Scientific Inc., USA) and open-path gas analyzers (LI-7500, LI-COR, USA) are combined to measure wind velocity, air temperature, water vapour and CO_2 concentrations at a frequency of 10 Hz. The azimuth angles of the three sonic anemometers are 110°, 120°, and 150° at 47, 140, and 280 m, respectively. Other instruments included sensors measuring hourly-averaged wind speed, wind direction, air temperature, and specific humidity at multiple heights ranging from 8 to 320 m.

Data processing includes linear detrending and density correction (Webb et al. 1980); the latter is applied to the instantaneous data following Detto and Katul (2007). In order to correct the tilt of the anemometer, the standard double-rotation method was compared to the planar fit method (Wilczak et al. 2001) that uses the whole dataset to determine a single plane representing the installed sonic alignment. Despite large pitch angles that were sometimes noted in the double-rotation methods, the two methods produce overall similar fluxes with correlation coefficients of determination always exceeding 0.86 when the averaging period is 1 h. In the following analysis, only results with the planar fit method are presented.

Friction velocity u_* is calculated following $u_* = \left(\overline{u'w'}^2 + \overline{v'w'}^2 \right)^{1/4}$, while sensible heat, latent heat, and carbon dioxide fluxes are respectively calculated following,

$$H = \rho C_p \overline{w'T'}, \tag{1}$$
$$L_v E = L_v \overline{w'\rho_v'}, \tag{2}$$
$$F_c = \overline{w'\rho_{CO_2}'}, \tag{3}$$

where u, v, and w are the streamwise, cross-stream, and vertical velocities (m s^{-1}), respectively, T is the air temperature (K), ρ_v is the water vapour density (kg m^{-3}), ρ_{CO_2} is the density of carbon dioxide (kg m^{-3}, not the density of carbon), ρ is the air density (kg m^{-3}), C_p and L_v are the specific heat capacity at constant pressure (J kg^{-1}K^{-1}) and the latent heat of vaporization of water (J kg^{-1}), respectively. The overbar denotes the Reynolds average, and the prime denotes the turbulent fluctuation from this average. The Obukhov length scale L (m) is calculated following

$$L = -\frac{\bar{T}u_*^3}{\kappa g \left(\overline{w'T'} + 0.61 \frac{\bar{T}}{\rho} \overline{w'\rho_v'} \right)} \tag{4}$$

where κ is the von Karman constant (0.4) and g is the acceleration due to gravity (9.81 m s^{-2}). Air density and specific humidity are first calculated based on the sonic-measured temperature, LICOR-measured water vapour concentration and pressure, and the sonic-measured temperature is then corrected to obtain air temperature. The above procedure is iterated until the calculated air temperature converges.

A few averaging periods are tested following the method used in Finnigan et al. (2003). When the averaging period changes from 0.5 to 1 h or from 1 to 2 h, the changes in momentum fluxes are small (within 3 %). When the averaging period increases from 0.5 to 1 h, the sensible heat flux is increased by 7 %, while the latent heat flux and CO_2 flux are decreased by 4 and 5 %, respectively. When the averaging period is further increased to 2 h, the sensible heat flux is further increased by an additional 1 %, while the latent heat flux and CO_2 flux are further decreased by additional 6 and 4 %, respectively. The optimal time period is difficult to determine: shorter times can filter flux contributions from larger motions and compromise the

Table 2 The number of segments at different levels under neutral, unstable and stable conditions

Heights (m)	Near-neutral	Unstable	Stable
47	360	438	29
140	50	671	57
280	8	276	114

statistical convergences of the Reynolds averages, while longer times can result in erroneously enhanced fluxes due to changes in the means at scales smaller than the averaging times (which add spurious turbulent perturbations). Therefore, an averaging period of 1 h is chosen in the following analysis as a compromise between these conflicting requirements.

Following Li and Bou-Zeid (2011), only data that satisfy the following criteria are used:

(1) wind directions face the sonic anemometers and the angle between the wind direction and the tower has to be smaller than $135°$;
(2) the variance of the velocity, temperature, and water vapour concentration for each segment is at least five times larger than the root-mean-square noise of the instrument as specified by the manufacturer so that the signal-to-noise ratio is sufficiently large;
(3) the absolute values of momentum and scalar fluxes must be larger than a threshold: $u_* > 0.1\,\mathrm{m\,s^{-1}}$, $|H| > 10\,\mathrm{W\,m^{-2}}$, $|L_v E| > 10\,\mathrm{W\,m^{-2}}$, and $|F_c| > 0.01\,\mathrm{mg\,m^{-2}\,s^{-1}}$ to ensure turbulent fluxes are well resolved by the instruments. Unusually large turbulent fluxes are also excluded from the analyses since they are likely to be associated with measurement problems such as spikes: sensible and latent heat fluxes should be within the range from $-200\,\mathrm{W\,m^{-2}}$ to $400\,\mathrm{W\,m^{-2}}$; the CO_2 flux should be within the range from $-2\,\mathrm{mg\,m^{-2}\,s^{-1}}$ to $4\,\mathrm{mg\,m^{-2}s^{-1}}$.

After the above procedures and filters are applied, the number of segments that remains is listed in Table 2. The near-neutral, unstable, and stable conditions are delineated based on the local stability parameter $(z - z_d)/L$, where z is the height of the measurement, z_d is the displacement height (= 5.4 m, see Al-Jiboori and Hu 2005 and Al-Jiboori 2008), and L is the local Obukhov length (computed with fluxes used at the given height). The use of a local L is required due to the large range of measurement heights. Many previous studies show that the local stability parameter $(z - z_d)/L$ can be used for roughness sublayer and/or mixed layer when turbulence statistics such as the standard deviations and the correlation coefficients are examined (Roth 1993; Roth and Oke 1993; Al-Jiboori et al. 2002; Christen et al. 2007; Al-Jiboori 2008; Wood et al. 2010). These studies involve different datasets collected over different urban surfaces, including datasets collected at this Beijing tower. As such, we also used the local stability parameter to separate the dataset into neutral conditions ($-0.2 < (z - z_d)/L < 0.2$), unstable conditions ($-10 < (z - z_d)/L < -0.2$) and stable conditions ($0.2 < (z - z_d)/L < 10$). In the analysis of transport efficiencies, we also used smaller bins in terms of the stability parameter (see Sect. 3.3).

Figure 3 displays wind roses at the three levels using the wind data measured by the sonic anemometers and filtered using the above procedures. As can be seen from Fig. 3, south and south-west directions are the most frequent during the analysis period (summer), which is due to the influence of the east Asian monsoon (see also Ding et al. 2008). From Fig. 2 it can be also seen that the southern part of the footprint, which is the area of the footprint contributing the most to the fluxes in view of these dominant wind directions, is generally more urbanized as compared to the northern part. Hence, it is expected that the dataset analyzed would mainly represent the characteristics associated with turbulent flows over highly urbanized areas, regardless of measurement height.

Fig. 3 Wind roses at the three levels (from *bottom to top* 47, 140, and 280 m)
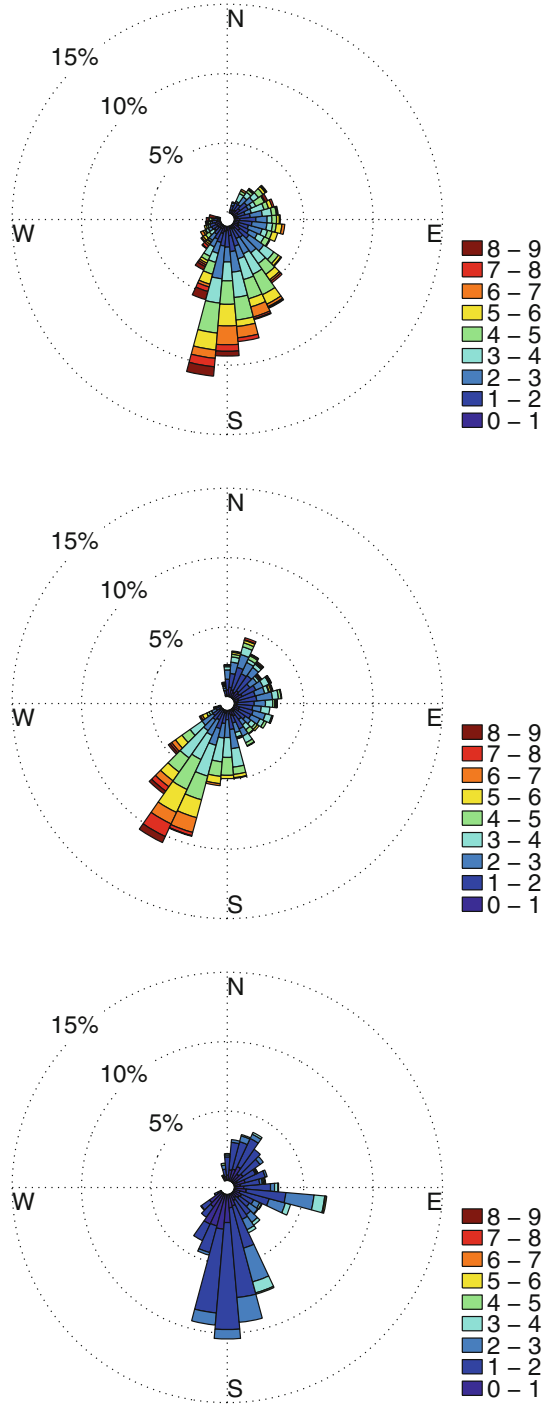
2.2 Quadrant Analysis and Characteristics of Ejection–Sweep Motions

Quadrant analysis has been widely used to identify and characterize coherent turbulent motions (Willmart and Lu 1972; Lu and Willmart 1973; Antonia 1981; Raupach 1981), and has also been applied to flow over vegetated canopies (see e.g., Shaw et al. 1983; Bergstrom and Hagstrom 1989; Gao et al. 1989; Paw et al. 1992; Katul and Cl 1997; Katul et al. 1997), as well as over urban canopies (Christen et al. 2007). We perform such an analysis here to probe the differences between the results for momentum and different scalars, and to assess the impact of stability on coherent motions over urban terrain.

Quadrant analysis separates the instantaneous momentum flux $(u'w')$ and scalar fluxes $(w'T', w'\rho'_v, w'\rho'_{CO_2})$ into four quadrants depending on the sign of two turbulent fluctuation components. The definition of each quadrant for momentum flux is as follows:

    quadrant 1: $u' > 0, w' > 0$, outward interactions,
    quadrant 2: $u' < 0, w' > 0$, ejections,
    quadrant 3: $u' < 0, w' < 0$, inward interactions,
    quadrant 4: $u' > 0, w' < 0$, sweeps.

As can be seen from the above definition, only fluxes from quadrants 2 and 4 (where $u'w' < 0$) contribute to the net downward momentum flux (which is the sum of the contributions from all four quadrants), while those from inward and outward interactions (quadrants 1 and 3) are counter-gradient fluxes that produce upward (positive) momentum flux and reduce the net downward momentum transport.

For scalars, the turbulent fluxes can be upward (positive) or downward (negative) depending on the bulk vertical gradients. Hence, following the same convention where ejections and sweeps contribute fluxes of the same sign as the dominant net flux, the definition of each quadrant for a scalar flux is:

    quadrant 1: $c' > 0, w' > 0$, ejection when $\overline{w'c'} > 0$; outward interactions when $\overline{w'c'} < 0$;
    quadrant 2: $c' < 0, w' > 0$, outward interactions when $\overline{w'c'} > 0$; ejection when $\overline{w'c'} < 0$;
    quadrant 3: $c' < 0, w' < 0$, sweep when $\overline{w'c'} > 0$; inward interactions when $\overline{w'c'} < 0$;
    quadrant 4: $c' > 0, w' < 0$, inward interactions when $\overline{w'c'} > 0$; sweep when $\overline{w'c'} < 0$;

where $c = T, \rho_v$ or ρ_{CO_2}. We note that when $\overline{w'c'} < 0$, the definition of the four quadrants is identical to that for momentum, while when $\overline{w'c'} > 0$ it is different. The consistent criterion in our definition is that ejections and sweeps are always the dominant eddy types for producing fluxes and they are of the same sign and direction as the net flux, but the quadrants that they occupy depend on the sign of the net flux during the averaging period. This is similar to the nomenclature used in Katul et al. (1997; 1997) and Francone et al. (2012); it is pointed out that ejection and sweep motions that produce negative scalar fluxes (for example, downward sensible heat flux or latent heat flux) are not well studied in urban environments where such downward scalar fluxes are less common than upward fluxes.

The characteristics of ejections and sweeps that are of particular interest to us are their flux contributions and time fractions. The flux contribution of each quadrant is defined as:

$$S(i) = \frac{\overline{w'a'}_i}{\overline{w'a'}}, \tag{5}$$

where

$$\overline{w'a'}_i = \frac{1}{T_a} \int_0^{T_a} w'a' I_i(t) \, dt, \tag{6}$$

where $a = u$ (horizontal velocity) or c (any scalar quantity), and i indicates the quadrant ($i = 1, 2, 3, 4$); T_a is the averaging period which is 1 h in our study, and

$$I_i = \begin{cases} 1 & if \ w'a' \ is \ in \ quadrant \ i \\ 0 & otherwise. \end{cases}$$

The time fraction of each quadrant is defined as

$$D(i) = \frac{1}{T_a} \int_0^{T_a} I_i(t)dt. \tag{7}$$

Statistical modelling of these characteristics of ejections and sweeps has been examined in many previous studies (Shaw et al. 1983; Katul and Cl 1997; Katul et al. 1997, 2006; Francone et al. 2012). A Gaussian joint probability density function (PDF) can be used to characterize the flux contributions and time fractions of the ejection–sweep motions (Katul and Cl 1997; Katul et al. 1997; Katsouvas et al. 2007). Assuming the flow variables are Gaussian-distributed, the flux contributions of ejections and sweeps are identical and can be described as (Katsouvas et al. 2007)

$$S_{\text{ejection}} = S_{\text{sweep}} = 0.25 + \frac{\left(-1 + 1/R_{wa}^2\right)^{0.5} + \arcsin\left(|R_{wa}|\right)}{2\pi}, \tag{8}$$

where $R_{wa} = \overline{w'a'}/(\sigma_w \sigma_a)$ is the correlation coefficient between w and a, and σ_w and σ_a are the standard deviations of w and a, respectively. Again, $a = u$ (horizontal velocity) or c (any scalar quantity). The time fractions of ejections and sweeps are given by (Katsouvas et al. 2007)

$$D_{\text{ejection}} = D_{\text{sweep}} = 0.25 + \frac{\arcsin\left(|R_{wa}|\right)}{2\pi}. \tag{9}$$

As shown in Eqs. 8 and 9, a Gaussian joint PDF results in equality between ejections and sweeps. As such, departures from a Gaussian joint PDF need to be taken into account in order to recover the often-observed unequal flux contributions and time fraction of ejections and sweeps. A third-order Gram–Charlier distribution is usually used to model the PDF of vertical velocity, horizontal velocity and scalars, and the cumulant expansion method (CEM) is used to predict the inequality between flux contributions from ejections and sweeps (Nakagawa and Nezu 1977; Raupach 1981; Shaw et al. 1983; Katul and Cl 1997). This results in a modified model where the relative importance of contributions from quadrant 4 (sweep for momentum and scalars when $\overline{w'c'} < 0$) and quadrant 2 (ejection for momentum and scalars when $\overline{w'c'} < 0$) is related to the third-order flow statistics through (Raupach 1981; Shaw et al. 1983)

$$\Delta S_o = S_{\text{sweep}} - S_{\text{ejection}} = \frac{1}{2 R_{wa} \sqrt{2\pi}} \left(\frac{1}{3} R_{wa} (M_{03} - M_{30}) + (M_{21} - M_{12})\right), \tag{10}$$

where M_{ij} are the dimensionless $(i + j)$ order joint moments given by

$$M_{ij} = \frac{\overline{(w')^i (a')^j}}{(\sigma_w)^i (\sigma_a)^j}. \tag{11}$$

In order to apply Eq. 10 to scalars when $\overline{w'c'} > 0$, a minor coordinate transformation is needed as discussed in Katul et al. (1997; 1997). Katul et al. (1997; 1997) also found that for

practical purposes $\frac{1}{3} R_{wa} (M_{03} - M_{30})$ is small relative to $(M_{21} - M_{12})$. As a result, Eq. 10 can be simplified to

$$\Delta S_{\mathrm{o}} = S_{\mathrm{sweep}} - S_{\mathrm{ejection}} = \frac{1}{2 R_{wa} \sqrt{2\pi}} (M_{21} - M_{12}). \tag{12}$$

Equation 12 is usually referred to as an incomplete cumulant expansion method (ICEM) due to the exclusion of the skewness terms M_{03} and M_{30}. Comparing CEM (Eq. 10) and ICEM (Eq. 12) suggests that only when the ratio $\frac{1}{3} R_{wa} (M_{03} - M_{30}) \big/ (M_{21} - M_{12})$ is small can the term $\frac{1}{3} R_{wa} (M_{03} - M_{30})$ be safely neglected. Through Eq. 12, the imbalance between ejections and sweeps in terms of the flux contribution is linked to the scalar variance budgets that involve variance transport terms like M_{12}. This ICEM has been demonstrated to work robustly over a variety of vegetated surfaces and under different stability conditions (Katul et al. 2006). However, it has not been tested over complex bluff urban canopies where the skewness of horizontal wind and scalars (M_{03}) can significantly deviate from that of the vertical wind (M_{30}) (see e.g., Graf et al. 2010; Böhm et al. 2012).

2.3 Turbulent Transport Efficiencies

The traditional transport efficiencies are usually defined based on the correlation coefficient

$$R_{wa} = \frac{\overline{w'a'}}{\sigma_w \sigma_a}. \tag{13}$$

Similar to Wyngaard and Moeng (1992), another measure of transport efficiency can also be defined as the ratio of the total flux divided by the flux that is transported downgradient by ejections and sweeps

$$\eta = \frac{F_{\mathrm{total}}}{F_{\mathrm{downgradient}}} = \frac{\overline{w'a'}_{\mathrm{total}}}{\overline{w'a'}_{\mathrm{ejection}} + \overline{w'a'}_{\mathrm{sweep}}}. \tag{14}$$

Note that in our definition, ejection and sweep events always act in the same direction as the net turbulent fluxes, while inward and outward interactions produce upgradient transport in the opposite direction to the net fluxes. As such, the transport efficiency defined above is always within the range of [0, 1]. This measure of transport efficiency can be analytically expressed as a function of the correlation coefficient R_{wa} when a Gaussian joint PDF is assumed (see Eq. 9 in Wyngaard and Moeng 1992).

3 Results and Discussions

3.1 Characteristics of Ejection–Sweep Motions

In this section, we examine the characteristics of ejection–sweep motions (i.e., flux contribution and time fraction) over the urban canopy using turbulence measurements at three different levels. Figure 4 shows the flux contributions from ejections and sweeps to the momentum flux, sensible heat flux, latent heat flux and CO_2 flux (from top to bottom) under stable, near-neutral, and unstable conditions (from left to right). The dots indicate the median values and the error bars denote the standard derivations over all available periods at each level (see Table 1). It is clear that the ejection–sweep motions have distinct flux contributions in different stability regimes. Under unstable conditions, ejections contribute more than sweeps
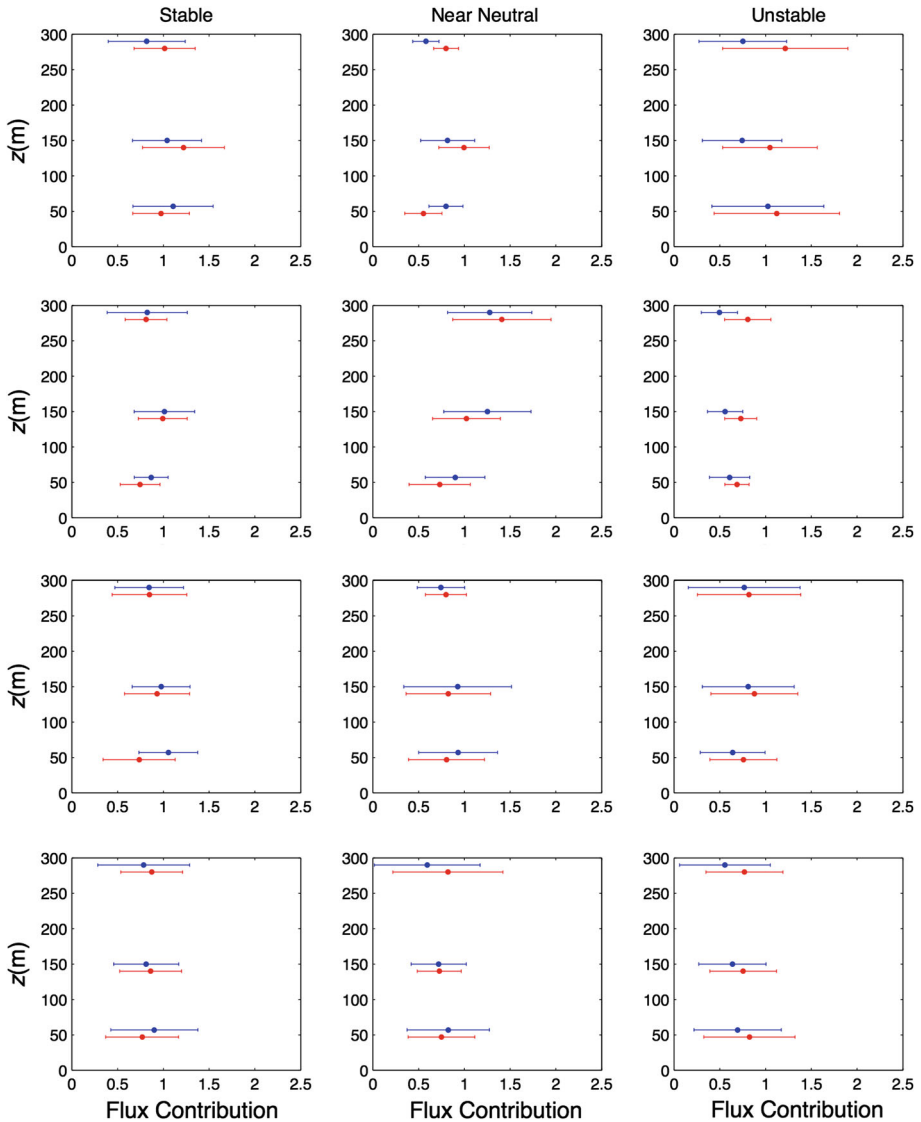
Fig. 4 Flux contributions from ejections (*red dots*) and sweeps (*blue dots*) to momentum flux, sensible heat flux, latent heat flux and CO_2 flux (respectively from *top to bottom*) under stable, near-neutral, and unstable conditions (respectively from *left to right*) at three levels (47, 140, and 280 m). The *blue dots* are shifted up by 10 m in order to compare with the *red dots*

to momentum flux, sensible heat flux, latent heat flux and CO_2 flux on average, which is in agreement with many previous studies that were conducted over a variety of surface types (Maitani and Ohtaki 1987; Maitani and Shaw 1990; Katul and Cl 1997; Katul et al. 1997; Moriwaki and Kanda 2006; Li and Bou-Zeid 2011; Dupont and Patton 2012; Francone et al. 2012). This is linked to the 'buoyantly-driven' structures or thermal plumes that are abundant under unstable conditions (see e.g., Paw et al. 1992; Li and Bou-Zeid 2011; Dupont and Patton 2012). Moriwaki and Kanda (2006) suggest that the ratios of flux contributions from

ejections to those from sweeps are highest for sensible heat flux and lowest for CO_2 flux under unstable conditions when the three scalars (i.e., temperature, water vapour and CO_2 concentration) are inter-compared. This is, however, not observed in our results. For example, the ratio of the flux contribution from ejections to that from sweeps is higher for the CO_2 flux than for the latent heat flux at 140 and 280 m. This underlines the role of urban morphology and surface composition, particularly the correlation of water vapour and CO_2 sources with those of sensible heat at the surface, in determining the ejection–sweep balance. The difference in the ratios of flux contributions is also linked to the difference in the turbulent transport efficiencies of water vapour and CO_2 (Moriwaki and Kanda 2006), as will be seen later.
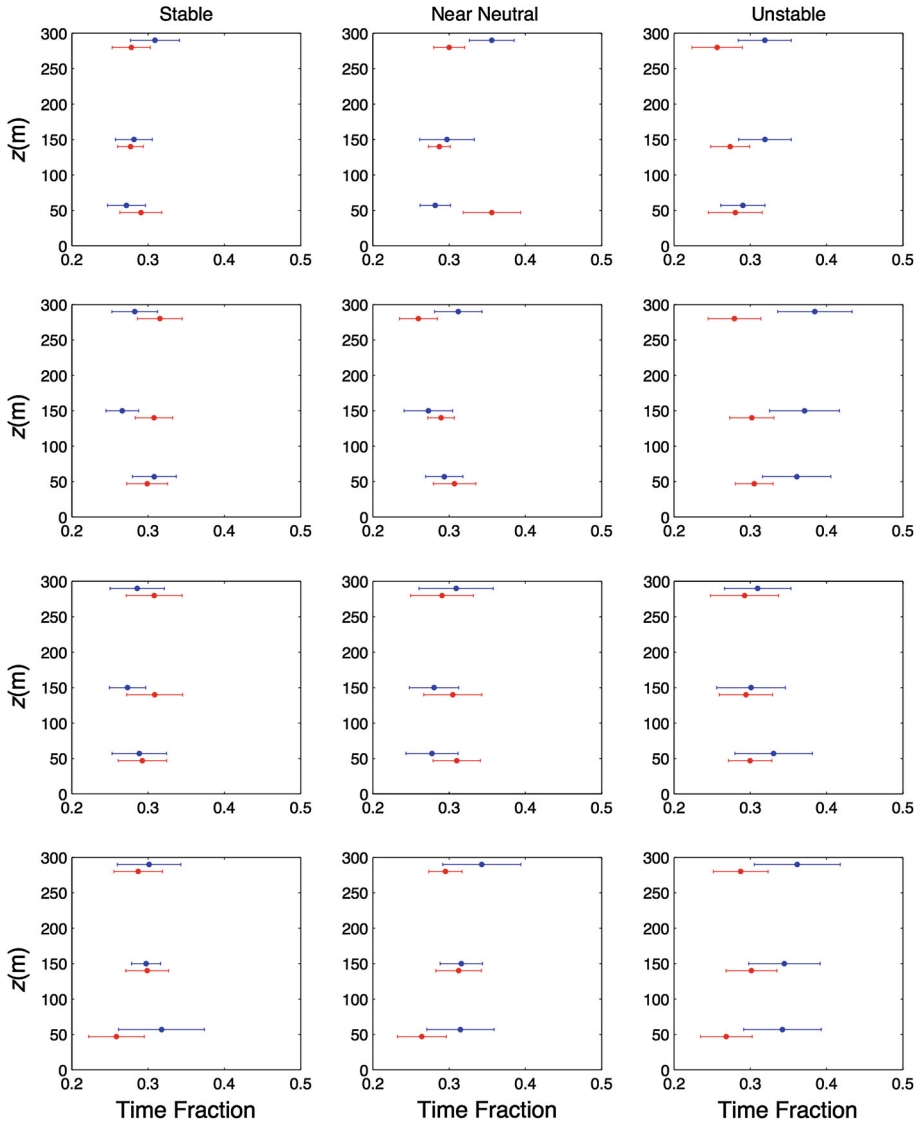
Under neutral and stable conditions, flux contributions from sweeps are larger than those from ejections at the lowest level (i.e., 47 m), which is within the urban roughness sublayer. Above the roughness sublayer, flux contributions from ejections become comparable to or exceed those from sweeps on average. This is also in agreement with previous studies that show sweeps dominate the momentum flux (see Shaw et al. 1983; Finnigan 2000; Poggi et al. 2004; Katul et al. 2006; Finnigan et al. 2009; Böhm et al. 2012) and the sensible heat flux (see Finnigan 2000; Christen et al. 2007; Dupont and Patton 2012) within canopies or roughness sublayers, while ejections dominate above the roughness sublayer. We also note that previous work has shown that the relative importance of ejections and sweeps changes with height within and above the roughness sublayer. Most of these studies are based on turbulence measurements/simulations within and/or above vegetation canopies (see Finnigan 2000 and Finnigan et al. 2009 for reviews), nevertheless, several studies were also conducted over real urban canopies (Christen et al. 2007) or over rough walls with bluff objects in wind tunnels (Coceal et al. 2007; Böhm et al. 2012). This suggests that the observation of sweeps-dominated momentum and scalar transports in the canopy or roughness sublayer under neutral or stable conditions holds for both vegetation and urban canopies.

The time fractions of ejections and sweeps are also notably different under different stability regimes, as can be seen from Fig. 5. Sweeps occupy more time compared to ejections under unstable conditions, suggesting that ejections are more intermittent, particularly for sensible heat flux and CO_2 flux. The fact that ejections contribute more to the fluxes (Fig. 4) while occupying less time (Fig. 5) clearly demonstrates that ejections are more efficient than sweeps under unstable conditions. This is again related to the 'buoyantly-driven' intense thermals under unstable conditions that are surrounded by slower subsiding columns of air and that are more efficient at transporting scalars than momentum (Li and Bou-Zeid 2011; Dupont and Patton 2012).

Under neutral and stable conditions, the time fractions of sweeps are slightly larger than those of ejections for CO_2 flux at all three levels, particularly at 47 m. However, for momentum flux, sensible heat and latent heat fluxes at 47 m, the time fractions of sweeps are less than or close to those of ejections. Given that the flux contribution of sweeps is larger than that of ejections (Fig. 4), while the time fraction of sweeps is less than or very close to that of ejections (Fig. 5) at 47 m, one can infer that sweeps transport momentum, sensible heat and latent heat more efficiently than ejections within the urban roughness sublayer. In addition, it also suggests that sweeps may transport CO_2 less efficiently than temperature and water vapour since the time fraction of sweeps is the largest for CO_2 among the three scalars. This is further examined using measures of turbulent transport efficiencies in Sect. 3.3.

3.2 Statistical Modelling of Ejection–Sweep Motions

In this section, the aim is to assess statistical models for characterizing ejection–sweep motions over an urban canopy. First, the Gaussian models for calculating the flux contributions

Fig. 5 Time fractions of ejections (*red dots*) and sweeps (*blue dots*) for momentum flux, sensible heat flux, latent heat flux and CO_2 flux (from *top to bottom*) under stable, near-neutral, and unstable conditions (from *left to right*) at three levels (47, 140, and 280 m). The *blue dots* are shifted up by 10 m in order to compare with the *red dots*

and time fractions of ejections and sweeps (Eqs. 8, 9) are evaluated. Under stable and near-neutral conditions, the Gaussian models reproduce the flux contributions and time fractions of ejections and sweeps fairly accurately for both momentum and scalar fluxes at all three levels (not shown). Under unstable conditions, however, departures from model predictions are occasionally seen, especially for scalar fluxes (not shown), which are caused by significant deviations of scalar PDFs from a Gaussian distribution (Chu et al. 1996; Liu et al. 2011). Previous studies also found that the skewness of scalars become increasingly larger than zero

as instability increases (Li and Bou-Zeid 2011). Given that the difference between the time fractions of ejections and sweeps is almost a linear function of the skewness (see Eq. 18 in Katul et al. 1997), the Gaussian models, which predict identical time fractions of ejections and sweeps, cannot capture the unequal time fractions of ejections and sweeps resulting from non-zero skewness of scalars.

The remainder of this section is focused on modelling the inequality between ejections and sweeps in terms of flux contributions as observed in Fig. 4. The difference in flux contributions between ejections and sweeps ($\Delta S_o = S_{ejection} - S_{sweep}$) is important given that it can be linked to the scalar variance budgets (Katul et al. 2006). The CEM and ICEM are used to model the difference in flux contributions from ejections and sweeps as functions of third-order cumulants ($M_{ij}, i + j = 3$). Since no significant qualitative difference is observed among the three levels, here only the results at 140 m are shown in Fig. 6. It appears that both CEM and ICEM yield reasonable estimates of the relative importance of ejections and sweeps, especially for the momentum flux (see the top panels of Fig. 6).

Table 3 presents a quantitative comparison between the results from the CEM and ICEM at all three levels for momentum and all scalars, including the simulated mean absolute ΔS_o, the ratio of the simulated and observed mean absolute ΔS_o, and the root-mean-square error ($RMSE$) between simulated and observed ΔS_o. Since ΔS_o can be either positive or negative, the modelled and observed mean values given in Table 3 are the mean of absolute ΔS_o. As one can see, the CEM and ICEM give slightly different mean values of absolute ΔS_o but the CEM does not necessarily produce better results when compared to observed mean ΔS_o. For example, the ratios of the simulated and observed mean absolute ΔS_o for momentum flux are closer to unity when the ICEM is used. Moreover, the $RMSE$ generated by the ICEM is sometimes smaller than that generated by the CEM, as suggested by the italicised values in Table 3. In summary, Table 3 suggests that the ICEM yields similar results as the CEM. One notable exception is associated with CO_2 at 47 m, where the ICEM generates a much larger $RMSE$ than does CEM and the ratio of the modelled and observed mean absolute ΔS_o from ICEM significantly deviates from unity.

It is of particular interest that the ICEM yields overall similar results as the CEM (Katul et al. 2006), suggesting that it is reasonable to ignore the contributions from the skewness terms in modelling the inequality between flux contributions from ejections and sweeps over bluff urban canopies. Figure 7 further examines this assumption by showing the cumulative distribution function (CDF) of the absolute value of $\frac{1}{3} R_{wa} (M_{03} - M_{30}) \big/ (M_{21} - M_{12})$. As mentioned earlier, only when this ratio is small can the term $\frac{1}{3} R_{wa} (M_{03} - M_{30})$ be safely neglected and the CEM and ICEM will generate similar results. As can be seen from Fig. 7, this is the case for momentum, temperature and water vapour at all three heights. For momentum, over 90 % of the segments have absolute values of this ratio < 0.5; for temperature and water vapour, about 80 % of the segments have absolute values of this ratio < 0.5. However, for CO_2, a large fraction of the segments have large absolute values of this ratio, in particular, at 47 m. This suggests that the skewness of CO_2 is significantly different from the skewness of vertical velocity. This is in agreement with the results shown in Table 3 that the ICEM generates a much larger $RMSE$ than does the CEM and the ratio of the modelled and observed mean absolute ΔS_o from the ICEM significantly deviates from unity for CO_2 at 47 m. Consequently, one can conclude that the ICEM fails for scalars such as CO_2 that have very different skewness from that of the vertical velocity, which can occur over heterogeneous surfaces such as the urban surface examined in this study.
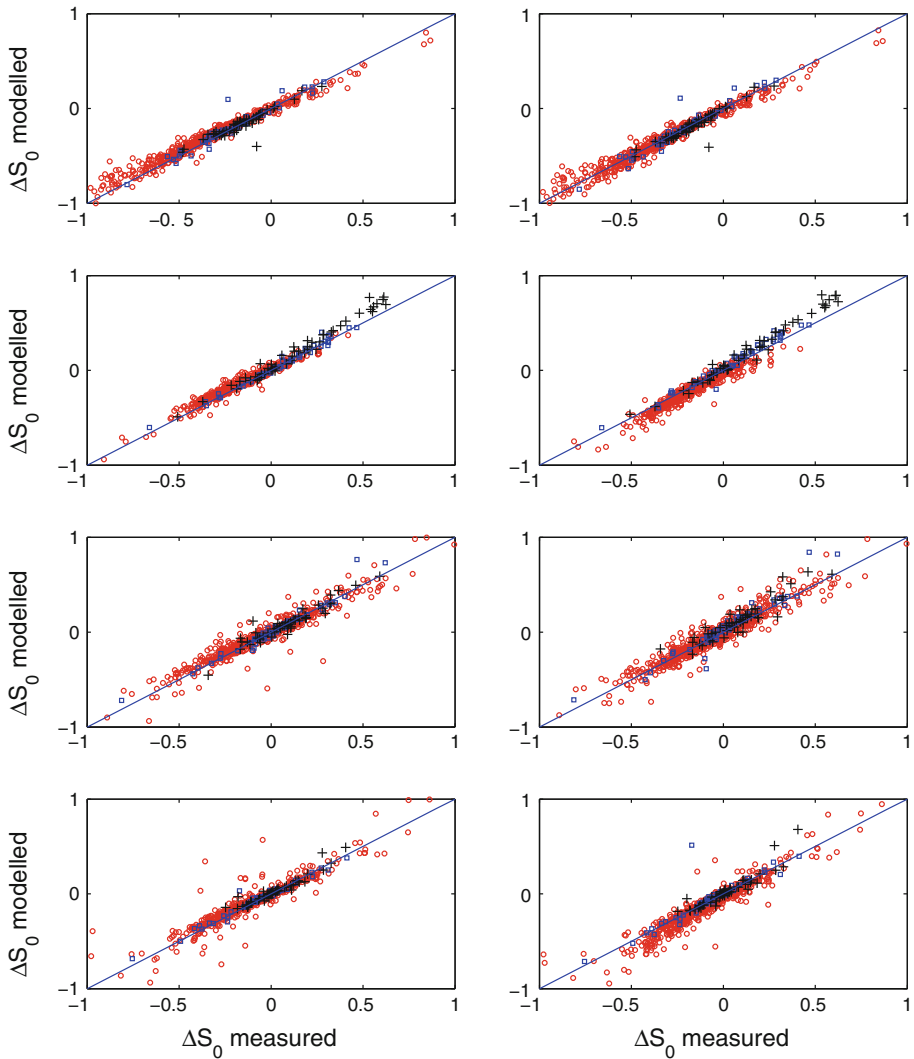
Fig. 6 Modelled and measured relative importance of ejections and sweeps for momentum flux, sensible heat flux, latent heat flux and CO_2 flux (from *top to bottom*) under neutral (*black pluses*), unstable (*red circles*) and stable (*blue squares*) conditions at 140 m. The *left panels* are using the CEM and the *right panels* are using the ICEM

3.3 Turbulent Transport Efficiencies of Momentum and Scalars

Previous sections examine the characteristics of coherent ejection–sweep motions where dissimilarity between momentum and scalars and among different scalars is observed. In this section, turbulent transport efficiencies are studied. Figure 8 shows the correlation coefficients (R_{uw}, R_{wT}, R_{wq}, R_{wCO_2}) at the three levels (from bottom to top: 47, 140, and 280 m). Also shown are some fitted functions proposed in the literature, some of which are based on experimental datasets collected over short, sparse vegetation surfaces (Bruin et al. 1993) and some of which are based on experimental datasets collected over tall, bluff urban canopies

Table 3 The modelled mean absolute ΔS_o values, the ratios of modelled and measured mean absolute ΔS_o values, and the root-mean-square errors *(RMSE)* of the modelled ΔS_o by CEM and ICEM

Height (m)	Momentum		Temperature		Water vapour		CO_2	
	CEM	ICEM	CEM	ICEM	CEM	ICEM	CEM	ICEM
	Mean							
47	0.24	0.27	0.19	0.21	0.17	0.20	0.21	0.28
140	0.30	0.33	0.17	0.21	0.17	0.18	0.15	0.19
280	0.34	0.38	0.25	0.32	0.18	0.20	0.22	0.26
	Ratio of means							
47	0.92	1.05	0.93	1.06	0.94	1.09	1.03	1.39
140	0.91	1.01	0.89	1.15	0.93	1.02	0.91	1.12
280	0.94	1.03	0.90	1.16	0.91	1.00	0.90	1.06
	RMSE							
47	0.003	0.004	0.001	0.003	0.002	0.004	0.015	0.038
140	0.004	*0.003*	0.002	0.004	0.005	0.006	0.006	0.006
280	0.006	0.006	0.032	*0.025*	0.006	0.008	0.013	*0.007*
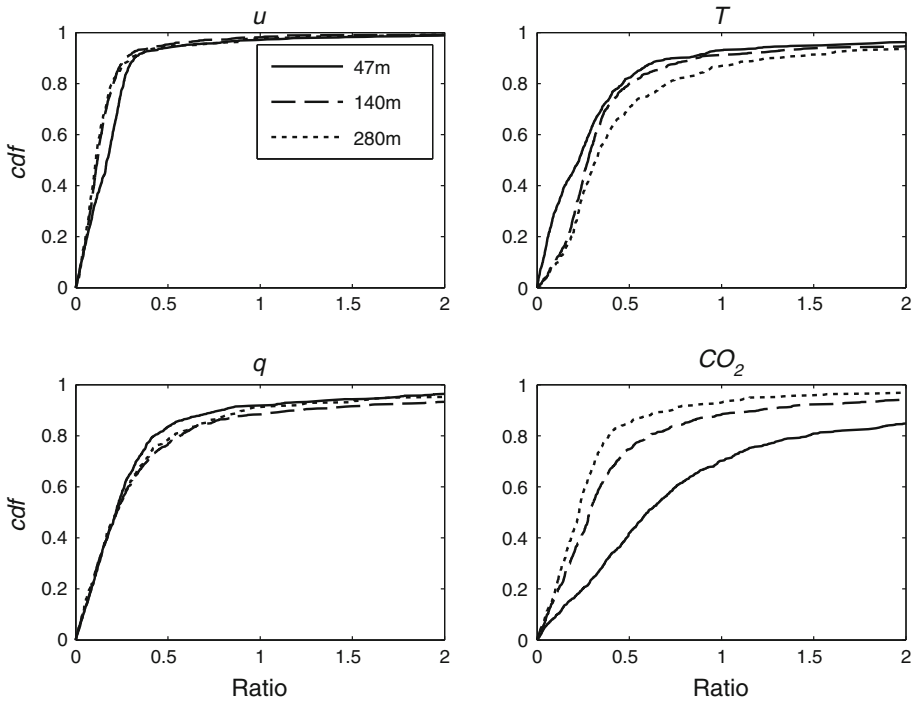
Fig. 7 The cumulative distribution function *(cdf)* of the ratio $\frac{1}{3} R_{wa} (M_{03} - M_{30}) \big/ (M_{21} - M_{12})$ for momentum, temperature, water vapour and CO_2 at the three heights

(Quan and Hu 2009; Wood et al. 2010). It needs to be pointed out that Quan and Hu (2009) also used a dataset collected at this Beijing tower, but only measurements at 47 m were considered and they did not explicitly consider the displacement height (z_d) in their fitting
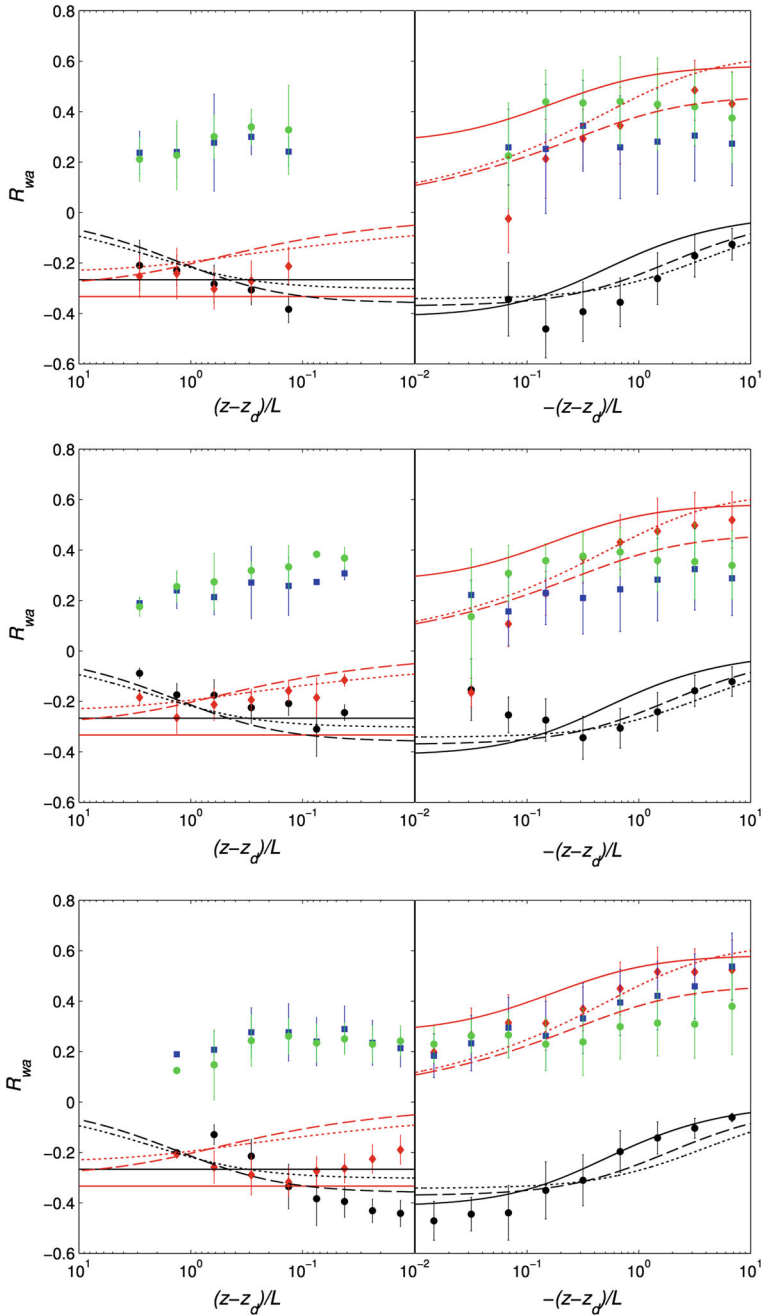
Fig. 8 Transport efficiencies of momentum and scalars under stable (*left panels*) and unstable (*right panel*) conditions at 47 m (*bottom panel*), 140 m (*middle panel*) and 280 m (*top panel*). The *vertical error bars* denote the standard deviation within each bin. The *solid lines* are fitted functions from Bruin et al. (1993); the *dashed lines* are fitted functions from Quan and Hu (2009) and the *dotted lines* are fitted functions from Wood et al. (2010)

process. Another difference is that when they calculated surface fluxes, only yaw rotation is conducted so that the x axis is aligned to the mean flow. Nevertheless, our analysis found that the pitch angle sometimes can be large due to either complex terrain or the fact that the sonic anemometer was not aligned exactly vertically. The fitted functions from Wood et al. (2010) are based on turbulence measurements at 190.3 m on a flux tower in London, UK, and the displacement height is considered when fitting a function for the transport efficiency.

Under unstable conditions ($0.2 < -(z - z_d)/L < 10$), there is a fair agreement between the observed turbulent transport efficiency for momentum and the fitted functions proposed in the literature, all of which indicate that the turbulent transport efficiency for momentum decreases as instability increases. Interestingly, the two fitted functions based on experimental datasets collected over urban canopies are below the fitted function over vegetation surfaces in this stability region, suggesting larger turbulent transport efficiencies for momentum over urban canopies (Roth 2000). The observed turbulent transport efficiencies for momentum at 140 and 280 m follow the fitted functions based on experimental datasets over urban canopies more closely, while the turbulent transport efficiency for momentum at 47 m seems to agree with the fitted function that is based on the experimental dataset over vegetation surface. Under near-neutral conditions ($-0.2 < (z - z_d)/L < 0.2$) and stable conditions ($0.2 < (z - z_d)/L < 10$), larger deviations from the fitted functions are observed. Under stable conditions, the transport efficiency of momentum clearly shows a decreasing trend with $(z - z_d)/L$ at all levels, which is in agreement with the two fitted functions proposed for urban surfaces, but is not predicted by the fitted function proposed for vegetated surfaces. Note that the fitted functions are not smooth at $(z - z_d)/L = 0$ as the atmosphere undergoes transition from unstable to stable, which is due to the fitting process as mentioned in Wood et al. (2010).
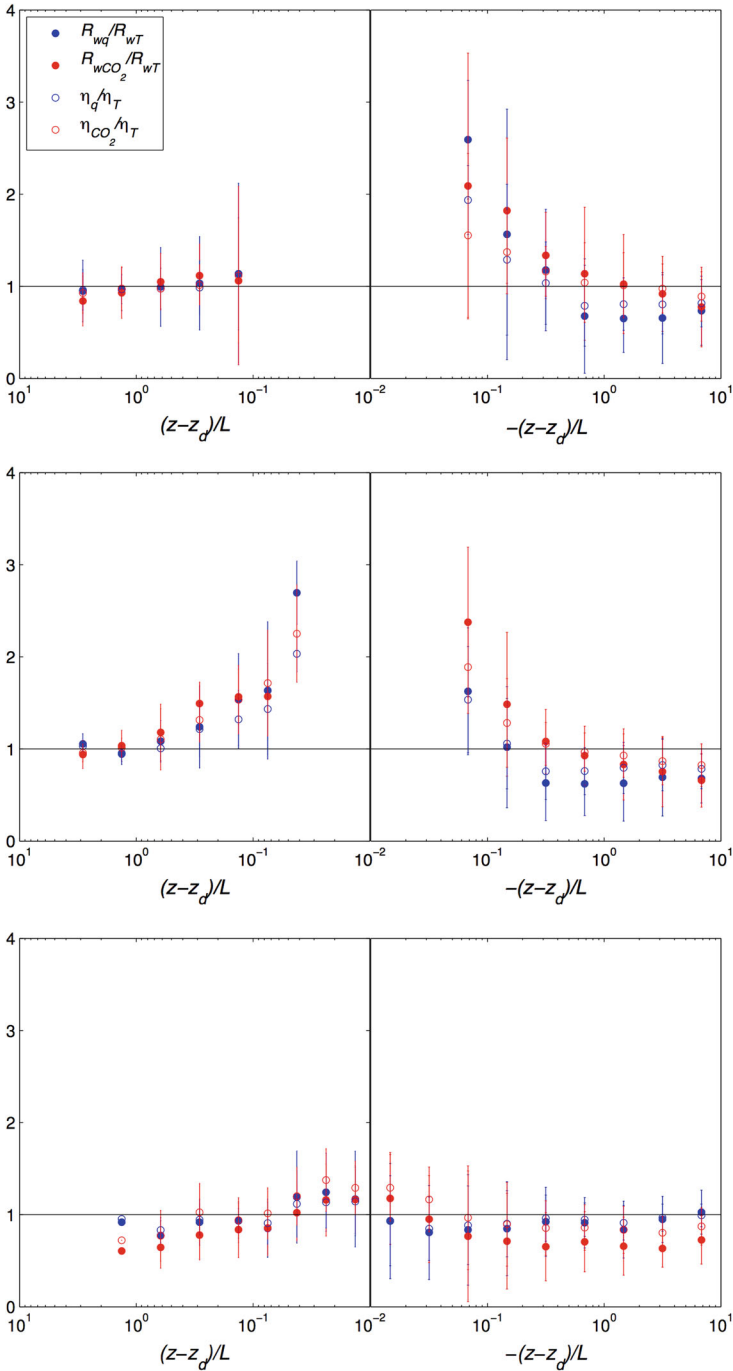
The transport efficiencies of scalars show significant differences from the transport efficiency of momentum. All fitted functions indicate that the transport efficiency of heat increase with $-(z - z_d)/L$ under unstable conditions, which is observed at the three levels. The two fitted functions for urban canopies also indicate that the transport efficiency of heat (the absolute magnitude) increases with $(z - z_d)/L$ under stable conditions, which is however not clearly observed. As such, the agreement between the measured transport efficiency of heat and the fitted functions (in particular the two functions for urban canopies) is satisfactory under unstable conditions, but not under stable conditions. The large variability of the transport efficiency of heat is not surprising given that the three fitted functions have already displayed large differences among each other.

It should be pointed out that the transport efficiencies of momentum and heat have self-correlations with the Obukhov length scale L. Nevertheless, the transport efficiencies of water vapour and CO_2 should not be affected by self-correlation. As can be seen from Fig. 8, the transport efficiencies of water vapour and CO_2 show distinct features as compared to the transport efficiency of heat. Despite their slight increase with atmosphere instability at 47 m under unstable conditions, they are almost unaltered by atmospheric instability at 140 and 280 m under both stable and unstable conditions, which is in agreement with Moriwaki and Kanda (2006). The transport efficiencies remain 0.2–0.4 with a slightly increasing trend observed as the atmosphere changes from stable to unstable conditions, indicating that these scalars are transported with equal efficiency by mechanical and buoyancy generated turbulence. These observations clearly indicate scalar dissimilarity, which is as expected over such a heterogeneous surface and suggest that many fitted functions proposed for the turbulent transport efficiency of heat cannot be simply extended for describing the turbulent transport efficiency of other scalars. Under stable conditions, the turbulent transport efficiency of heat becomes negative due to the downward heat fluxes; nevertheless, the turbulent transport effi-

ciencies of water vapour and CO_2 remain positive, implying that the latent heat flux and CO_2 flux are upward even under stable conditions. When the absolute magnitudes are considered, the turbulent transport efficiencies of water vapour and CO_2 are comparable to that of temperature under stable conditions, as shall be seen later. The dissimilarity seen among the three scalars is further investigated by examining the ratios of these transport efficiencies.

Figure 9 shows the ratios of transport efficiencies of water vapour and CO_2 to the transport efficiency of temperature, where the signs of transport efficiencies are not considered. When the ratios < 1, heat is transported more efficiently than water vapour and CO_2, and vice versa. Two different measures of transport efficiencies, the correlation coefficient and the efficiency based on flux contributions from ejections and sweeps, are both shown on Fig. 9. As one can see, the two measures of transport efficiencies yield similar patterns and trends despite of differences in the magnitude. Under very unstable conditions, the ratios are generally <1, implying that heat is transported more efficiently than other scalars. This has been observed and analyzed by many previous studies (Warhaft 1976; Katul and Parlange 1994; Katul and Cl 1999; Assouline et al. 2008; Li et al. 2012; Zhao et al. 2013). The buoyant production term in the sensible heat flux budget equation is always more significant than that in the water vapour/CO_2 flux budget equations. As the atmosphere tends towards neutral, temperature fluctuations can be easily generated by horizontal temperature gradients, which result in an increase in the temperature variance and a concomitant reduction in the transport efficiency (see also Nordbo et al. 2013). This effect is less prominent for inactive scalars such as water vapour and CO_2, and as a result, the ratios of transport efficiencies of water vapour and CO_2 to the transport efficacy of temperature increase. Note that, although water vapour can modify the dynamics of the atmospheric flow to a certain degree, it is usually viewed as an inactive scalar rather than an active scalar. Under stable conditions, the transport efficiencies of the three scalars are similar at 140 and 280 m, implying scalar similarity under stable conditions (Dias and Brutsaert 1996). The ratio being ≈ 1 at 280 m might suggest that turbulence is very weak and the height of the stable ABL is below 280 m. At 47 m, heat is transported more efficiently than the other two scalars, and the transport efficiency of water vapour is slightly higher than that of CO_2 and is thus closer to that of heat. The lower transport efficiency of CO_2 observed at 47 m under stable conditions is in agreement with the larger time fractions of sweeps as observed in Fig. 5. Our findings are nonetheless not in agreement with Nordbo et al. (2013) who observed that heat is always transported less efficiently than water vapour and CO_2 under stable conditions. This highlights the need of further investigation on turbulent transports of scalars over urban canopies under stable conditions.

The differences seen between temperature and the other two inactive scalars can also be induced through the surface heterogeneity effect (i.e., the sources and sinks for scalars are different). As suggested by Moriwaki and Kanda (2006), some thermal structures that transport heat under unstable conditions may also transport water vapour and CO_2 but others may not due to the mismatch between the location of a thermal structure and the region of high water vapour or CO_2 concentration. In addition, the heterogeneity of sources and sinks can also produce dissimilarity between water vapour and CO_2 (Moriwaki and Kanda 2006; Williams et al. 2007; Nordbo et al. 2013). Moriwaki and Kanda (2004) show that the main source of water vapour over a residential area in Tokyo, Japan is vegetation transpiration, while the main source of CO_2 is the consumption of fossil fuels, from both vehicles, home heating, and the exhalations of humans. Around the Beijing tower, the fraction of vegetation and soil is not negligible and the latent heat flux in summer months is of comparable magnitude to that observed by Moriwaki and Kanda (2004) (see e.g., Miao et al. 2012). Some studies also suggest that the major source of CO_2 in Beijing is transportation and heating/cooling (Liu et al. 2012; Song and Wang 2012). As such, the dissimilarity between water vapour

Fig. 9 Ratios of transport efficiencies of water vapour and CO_2 to the transport efficacy of heat under stable (*left panels*) and unstable (*right panels*) conditions at 47 m (*bottom panel*), 140 m (*middle panel*) and 280 m (*top panel*). The *vertical error bars* denote the standard deviation within each bin

and CO_2 is expected, which is indeed observed in Fig. 9. Nevertheless, it is interesting to observe that at 47 m, the transport of water vapour is more efficient than CO_2 under unstable conditions while the opposite is true at 140 and 280 m. Moriwaki and Kanda (2006) and Nordbo et al. (2013) also observed a higher transport efficiency for water vapour than CO_2 under unstable conditions. The height at which turbulence measurements used in Moriwaki and Kanda (2006) is taken is 29 m, and the three eddy-covariance stations employed in the study of Nordbo et al. (2013) have heights of 31, 41.8, and 60 m. As such, our observation that water vapour is transported more efficiently at 47 m under unstable conditions is in agreement with these two studies. At higher levels, the turbulent transport is also affected by advection, top–down diffusion, and other large-scale processes that may also induce scalar dissimilarity (see e.g., McNaughton and Laubach 1998; Lee et al. 2004; Asanuma et al. 2007; Cava et al. 2008; Katul et al. 2008; Huang et al. 2009; Li et al. 2012).

4 Conclusions

Turbulence measurements available at the Beijing's 325 m flux tower (at 47, 140 and 280 m) provide valuable opportunities to examine turbulent structures over extremely rough and heterogeneous surfaces in the atmospheric boundary layer. In this study, the quadrant analysis technique is used to examine the turbulent transport of momentum, temperature, water vapour and CO_2. The characteristics of ejection–sweep motions are quantified, and it is found that the ejection–sweep motions at all three levels are strongly affected by the atmospheric stability. Under unstable conditions, ejections contribute more to the total fluxes than do sweeps but occupy less time, which is linked to the 'buoyantly-driven' structures or thermal plumes. Under neutral and stable conditions, sweeps dominate momentum transfer and scalar transfer at the lowest level, which is within the urban roughness sublayer.

Modelling of the characteristics of ejections and sweeps such as flux contributions and time fractions is also investigated in this study. A Gaussian joint probability density function for flow variables is sufficient to reproduce the flux contributions and time fractions of ejections and sweeps. Nevertheless, in order to capture the unequal flux contributions from ejections and sweeps, third-order statistics have to be included. The third-order cumulant expansion method (CEM) and the truncated incomplete cumulant expansion method (ICEM) both reasonably reproduce the imbalance between flux contributions from ejections and sweeps. However, the ICEM is not applicable for CO_2 at 47 m due to the fact that CO_2 at 47 m has a significantly larger skewness than vertical velocity.

Dissimilarity between momentum and scalar transfer is observed in the characteristics of ejection–sweep motions. For example, the flux contributions and time fractions of ejections and sweeps are different for momentum and scalars. The relative importance of ejections and sweeps is also different for momentum and scalars. The time fractions of sweeps at 47 m are slightly larger than those of ejections for CO_2 flux but smaller than or close to those of ejections for momentum, heat and water vapour fluxes. The departures of the characteristics of ejections and sweeps from Gaussian model predictions are larger for scalars than for momentum under unstable conditions. As compared to the CEM, the ICEM also reproduces the imbalance between contributions from ejections and sweeps for the momentum flux; nevertheless, the ICEM does not work well for CO_2 at 47 m due to the breakdown of its assumption. These dissimilarities in the characteristics of turbulent structures are strongly linked to the different transport efficiencies of momentum and scalars.

A transport efficiency measure based on quadrant analysis, together with the traditional transport efficiency measure based on the correlation coefficient, are used to quantify the

dissimilarity between the turbulent transport of momentum and scalars. The results indicate that atmospheric stability has important effects on transport efficiencies of momentum and heat; under unstable conditions, the transport efficiency of momentum decreases as instability increases while the transport efficiency of heat increases; under stable conditions, the transport efficiency of momentum decreases while the transport efficiency of heat does not display a clear trend. The transport efficiencies of momentum and heat are also compared to fitted functions from three previous studies of which two are based on experimental datasets over urban canopies. Our results are in broad agreement with these studies, particularly for momentum. Nevertheless, some discrepancies are observed under near-neutral and stable conditions.

Compared to the transport efficiency of heat, the transport efficiencies of water vapour and CO_2 are not significantly altered by the atmospheric stability. The dissimilarity among the three scalars is further examined using the ratios of transport efficiencies of water vapour and CO_2 to the transport efficiency of heat. Under very unstable conditions, heat is transported more efficiently than is water vapour and CO_2, which is in agreement with many previous studies. As the atmosphere tends towards neutral, the ratios increase due to a significant decrease in the transport efficiency of heat. Under very stable conditions, the three scalars are transported similarly at 140 and 280 m; at 47 m, the transport of water vapour is more efficient than that of CO_2, which is in agreement with the finding that the time fractions of sweeps are larger for CO_2 given that sweeps are the dominant mechanism for scalar transport in the roughness sublayer. The dissimilarity among scalars is caused by the combination of the active role of temperature and the surface heterogeneity effect.

There are some limitations of this study that are important to appreciate. First, the results are based on measurements at three levels but it is well-known that turbulence changes significantly with heights even within the same layer as shown in Fig. 1. As such, the results might not represent the whole picture of a given layer. Second, the sources and sinks for scalars are likely to vary seasonally and annually. The rapid urbanization in Beijing can also lead to changes in the surface properties, which will affect the turbulent transport of momentum and scalars within and above the urban canopy. These effects are not considered here but may be important for other applications.

References

AI-Jiboori MH (2008) Correlation coefficients in urban turbulence. Boundary-Layer Meteorol 126(2):311–323

AI-Jiboori MH, Hu F (2005) Surface roughness around a 325-m meteorological tower and its effect on urban turbulence. Adv Atmos Sci 22(4):595–605

AI-Jiboori MH, Xu YM, Qian YF (2002) Local similarity relationships in the urban boundary layer. Boundary-Layer Meteorol 102(1):63–82

Antonia RA (1981) Conditional sampling in turbulence measurement. Annu Rev Fluid Mech 13:131–156

Arnfield AJ (2003) Two decades of urban climate research: a review of turbulence, exchanges of energy and water, and the urban heat island. lnt J Climatol 23(1):1–26

Asanuma J, Tamagawa I, Ishikawa H, Ma YM, Hayashi T, Qi YQ, Wang JM (2007) Spectral similarity between scalars at very low frequencies in the unstable atmospheric surface layer over the Tibetan plateau. Boundary-Layer Meteorol 122(1):85–103

Assouline S, Tyler SW, Tanny J, Cohen S, Bou-Zeid E, Parlange MB, Katul GG (2008) Evaporation from three water bodies of different sizes and climates: measurements and scaling analysis. Adv Water Resour 31(1):160–172

Bergstrom H, Hagstrom U (1989) Turbulent exchange above a Pine forest.2. Organized structures. Boundary-Layer Meteorol 49(3):231–263

Böhm M, Finnigan J, Raupach M, Hughes D (2012) Turbulence structure within and above a canopy of bluff elements. Boundary-Layer Meteorol 1–27

Britter RE, Hanna SR (2003) Flow and dispersion in urban areas. Annu Rev Fluid Mech 35:469–496

Brutsaert W (1982) Evaporation into the atmosphere: theory, history, and applications. Reidel, Dordrecht, Holland

Cava D, Katul GG, Sempreviva AM, Giostra U, Scrimieri A (2008) On the anomalous behaviour of scalar flux-variance similarity functions within the canopy sub-layer of a dense alpine forest. Boundary-Layer Meteorol 128(1):33–57

Chen F, Kusaka H, Bornstein R, Ching J, Grimmond CSB, Grossman-Clarke S, Loridan T, Manning KW, Martilli A, Miao SG, Sailor D, Salamanca FP, Taha H, Tewari M, Wang XM, Wyszogrodzki AA, Zhang CL (2011) The integrated WRF/urban modelling system: development, evaluation, and applications to urban environmental problems. lnt J Climatol 31(2):273–288

Christen A, Rotach MW, Vogt R (2009) The budget of turbulent kinetic energy in the urban roughness sublayer. Boundary-Layer Meteorol 131(2):193–222

Christen A, van Gorsel E, Vogt R (2007) Coherent structures in urban roughness sublayer turbulence. lnt J Climatol 27(14):1955–1968

Chu CR, Parlange MB, Katul GG, Albertson JD (1996) Probability density functions of turbulent velocity and temperature in the atmospheric surface layer. Water Resour Res 32(6):1681–1688

Coceal O, Dobre A, Thomas TG, Belcher SE (2007) Structure of turbulent flow over regular arrays of cubical roughness. J Fluid Mech 589:375–409

De Bruin HAR, Kohsiek W, Vandenhurk BJJM (1993) A verification of some methods to determine the fluxes of momentum, sensible heat, and water-vapor using standard-deviation and structure parameter of scalar meteorological quantities. Boundary-Layer Meteorol 63(3):231–257

De Bruin HAR, Van Den Hurk B, Kroon UM (1999) On the temperature-humidity correlation and similarity. Boundary-Layer Meteorol 93(3):453–468

Detto M, Katul G, Mancini M, Montaldo N, Albertson JD (2008) Surface heterogeneity and its signature in higher-order scalar similarity relationships. Agric For Meteorol 148(6–7):902–916

Detto M, Katul GG (2007) Simplified expressions for adjusting higher-order turbulent statistics obtained from open path gas analyzers. Boundary-Layer Meteorol 122(1):205–216

Dias NL, Brutsaert W (1996) Similarity of scalars under stable conditions. Boundary-Layer Meteorol 80(4):355–373

Ding AJ, Wang T, Thouret V, Cammas JP, Nedelec P (2008) Tropospheric ozone climatology over Beijing: analysis of aircraft data from the MOZAIC program. Atmos Chern Phys 8(1):1–13

Dupont S, Patton EG (2012) Momentum and scalar transport within a vegetation canopy following atmospheric stability and seasonal canopy changes: the CHATS experiment. Atmos Chern Phys 12(13):5913–5935

Feigenwinter C, Vogt R (2005) Detection and analysis of coherent structures in urban turbulence. Theor Appl Climatol 81(3–4):219–230

Fernando HJS (2010) Fluid Dynamics of Urban Atmospheres in Complex Terrain. Annu Rev Fluid Mech 42:365–389

Fernando HJS, Zajic D, DiSabatino S, Dimitrova R, Hedquist B, Dallman A (2010) Flow, turbulence, and pollutant dispersion in urban atmospheres. Phys Fluids 22(5)

Finnigan J (2000) Turbulence in plant canopies. Annu Rev Fluid Mech 32:519–571

Finnigan JJ, Clement R, Malhi Y, Leuning R, Cleugh HA (2003) A re-evaluation of long-term flux measurement techniques: Part 1: averaging and coordinate rotation. Boundary-Layer Meteorol 107(1):1–48

Finnigan JJ, Shaw RH, Patton EG (2009) Turbulence structure above a vegetation canopy. J Fluid Mech 637:387–424

Francone C, Katul GG, Cassardo C, Richiardone R (2012) Turbulent transport efficiency and the ejection-sweep motion for momentum and heat on sloping terrain covered with vineyards. Agric For Meteorol 162:98–107

Gao W, Shaw RH, Paw KT (1989) Observation of organized structure in turbulent-flow within and above a forest canopy. Boundary-Layer Meteorol 47(1–4):349–377

Graf A, Schuttemeyer D, Geiss H, Knaps A, Mollmann-Coers M, Schween JH, Kollet S, Neininger B, Herbst M, Vereecken H (2010) Boundedness of turbulent temperature probability distributions, and their relation to the vertical profile in the convective boundary layer. Boundary-Layer Meteorol 134(3):459–486

Grimm NB, Faeth SH, Golubiewski NE, Redman CL, Wu JG, Bai XM, Briggs JM (2008) Global change and the ecology of cities. Science 319(5864):756–760

Grimmond CSB, Blackett M, Best MJ, Bail JJ, Belcher SE, Beringer J, Bohnenstengel 51, Calmet I, Chen F, Coutts A, Dandou A, Fortuniak K, Gouvea ML, Hamdi R, Hendry M, Kanda M, Kawai T, Kawamoto Y, Kondo H, Krayenhoff ES, Lee SH, Loridan T, MartiIIi A, Masson V, Miao S, Oleson K, Ooka R, Pigeon G, Parson A, Ryu YH, Salamanca F, Steeneveld GJ, Tombrou M, Voogt JA, Young DT, Zhang N (2011) Initial results from Phase 2 of the international urban energy balance model comparison. lnter J Climatol 31(2):244–272

Grimmond CSB, Blackett M, Best MJ, Barlow J, Baik JJ, Belcher SE, Bohnenstengel 51, Calmet I, Chen F, Dandou A, Fortuniak K, Gouvea ML, Hamdi R, Hendry M, Kawai T, Kawamoto Y, Kondo H, Krayenhoff ES, Lee SH, Loridan T, Martilli A, Masson V, Miao S, Oleson K, Pigeon G, Parson A, Ryu YH, Salamanca F, Shashua-Bar L, Steeneveld GJ, Tombrou M, Voogt J, Young D, Zhang N (2010) The international urban energy balance models comparison project: first results from phase 1. J Appl Meteorol Clim 49(6):1268–1292

Grimmond CSB, Oke TR (2002) Turbulent heat fluxes in urban areas: Observations and a local-scale urban meteorological parameterization scheme (LUMPS). J Appl Meteorol 41(7):792–810

Horiguchi M, Hayashi T, Hashiguchi H, Ito Y, Ueda H (2010) Observations of coherent turbulence structures in the near-neutral atmospheric boundary layer. Boundary-Layer Meteorol 136(1):25–44

Hou A, Ni G, Yang H, Lei Z (2013) Numerical analysis on the contribution of urbanization to wind stilling. an example over the greater Beijing metropolitan area. J Appl Meteorol Clim 52(5):1105–1115. doi:10.1175/JAMC-D-12-013.1

Huang JP, Lee XH, Patton EG (2009) Dissimilarity of scalar transport in the convective boundary layer in inhomogeneous landscapes. Boundary-Layer Meteorol 130(3):327–345

lnagaki A, Kanda M (2010) Organized structure of active turbulence over an array of cubes within the logarithmic layer of atmospheric flow. Boundary-Layer Meteorol 135(2):209–228

Iwata H, Harazono Y, Ueyama M (2010) Influence of source/sink distributions on flux-gradient relationships in the roughness sublayer over an open forest canopy under unstable conditions. Boundary-Layer Meteorol 136(3):391–405

Kanda M (2006) Large-eddy simulations on the effects of surface geometry of building arrays on turbulent organized structures. Boundary-Layer Meteorol 118(1):151–168

Kanda M, Moriwaki R, Kasamatsu F (2004) Large-eddy simulation of turbulent organized structures within and above explicitly resolved cube arrays. Boundary-Layer Meteorol 112(2):343–368

Katsouvas GD, Helmis CG, Wang Q (2007) Quadrant analysis of the scalar and momentum fluxes in the stable marine atmospheric surface layer. Boundary-Layer Meteorol 124(3):335–360

Katul G, Cl Hsieh (1997a) Turbulent eddy motion at the forest-atmosphere interface. J Geophys Res Atmos 102(D12):13409–13421

Katul G, Kuhn G, Schieldge J, Cl Hsieh (1997b) The ejection-sweep character of scalar fluxes in the unstable surface layer. Boundary-Layer Meteorol 83(1):1–26

Katul G, Poggi D, Cava D, Finnigan J (2006) The relative importance of ejections and sweeps to momentum transfer in the atmospheric boundary layer. Boundary-Layer Meteorol 120(3):367–375

Katul GG, Cl Hsieh (1999) A note on the flux-variance similarity relationships for heat and water vapour in the unstable atmospheric surface layer. Boundary-Layer Meteorol 90(2):327–338

Katul GG, Parlange MB (1994) On the active-role of temperature in surface-layer turbulence. J Atmos Sci 51(15):2181–2195

Katul GG, Sempreviva AM, Cava D (2008) The temperature-humidity covariance in the marine surface layer: a one-dimensional analytical model. Boundary-Layer Meteorol 126(2):263–278

Lee X, Yu Q, Sun X, Liu J, Min Q, Liu Y, Zhang X (2004) Micrometeorological fluxes under the influence of regional and local advection: a revisit. Agric For Meteorol 122(1–2):111–124

Li D, Bou-Zeid E (2011) Coherent structures and the dissimilarity of turbulent transport of momentum and scalars in the unstable atmospheric surface layer. Boundary-Layer Meteorol 140(2):243–262

Li D, Bou-Zeid E, De Bruin H (2012a) Monin-Qbukhov similarity functions for the structure parameters of temperature and humidity. Boundary-Layer Meteorol 145(1):45–67

Li D, Katul GG, Bou-Zeid E (2012b) Mean velocity and temperature profiles in a sheared diabatic turbulent boundary layer. Phys Fluids 24(10)

Li QS, Zhi LH, Hu F (2010) Boundary layer wind structure from observations on a 325m tower. J Wind Eng lnd Aerodyn 98(12):818–832

Liu HZ, Feng JW, Jarvi L, Vesala T (2012) Four-year (2006–2009) eddy covariance measurements of CO_2 flux over an urban area in Beijing. Atmos Chern Phys 12(17):7881–7892

Liu L, Hu F, Cheng XL (2011) Probability density functions of turbulent velocity and temperature fluctuations in the unstable atmospheric surface layer. J Geophys Res Atmos 116

Lu SS, Willmart WW (1973) Measurements of structure of reynolds stress in a turbulent boundary-layer. J Fluid Mech 60(Sep18):481–511

Maitani T, Ohtaki E (1987) Turbulent transport processes of momentum and sensible heat in the surface-layer over a paddy field. Boundary-Layer Meteorol 40(3):283–293

Maitani T, Shaw RH (1990) Joint probability analysis of momentum and heat fluxes at a deciduous forest. Boundary-Layer Meteorol 52(3):283–300

Marusic I, McKeon BJ, Monkewitz PA, Nagib HM, Smits AJ, Sreenivasan KR (2010) Wall-bounded turbulent flows at high Reynolds numbers: recent advances and key issues. Phys Fluids 22(6):065103

McNaughton KG, Laubach J (1998) Unsteadiness as a cause of non-equality of eddy diffusivities for heat and vapour at the base of an advective inversion. Boundary-Layer Meteorol 88(3):479–504

Miao S, Dou J, Chen F, Li J, Li A (2012) Analysis of observations on the urban surface energy balance in Beijing. Sci China Earth Sci 55(11):1881–1890

Moene AF, Schuttemeyer D (2008) The effect of surface heterogeneity on the temperature-humidity correlation and the relative transport efficiency. Boundary-Layer Meteorol 129(1):99–113

Moriwaki R, Kanda M (2004) Seasonal and diurnal fluxes of radiation, heat, water vapor, and carbon dioxide over a suburban area. J Appl Meteorol 43(11):1700–1710

Moriwaki R, Kanda M (2006) Local and global similarity in turbulent transfer of heat, water vapour, and CO_2 in the dynamic convective sublayer over a suburban area. Boundary-Layer Meteorol 120(1):163–179

Nakagawa H, Nezu I (1977) Prediction of contributions to reynolds stress from bursting events in open-channel flows. J Fluid Mech 80(Apr4):99–128

Nordbo A, Jarvi L, Haapanala S, Moilanen J, Vesala T (2013) Intra-city variation in urban morphology and turbulence structure in helsinki, finland. Boundary-Layer Meteorol 146(3):469–496

Oke TR (1988) The urban energy-balance. Prog Phys Geogr 12(4):471–508

Paw KT, Brunet Y, Collineau S, Shaw RH, Maitani T, Qiu J, Hipps L (1992) On coherent structures in turbulence above and within agricultural plant canopies. Agric For Meteorol 61(1–2):55–68

Piringer M, Grimmond CSB, Joffre SM, Mestayer P, Middleton DR, Rotach MW, Baklanov A, De Ridder K, Ferreira J, Guilloteau E, Karppinen A, Martilli A, Masson V, Tombrou M (2002) Investigating the surface energy balance in urban areas- recent advances and future needs. Water Air Soil Pollut Focus 2(5–6):1–16

Poggi D, Porporato A, Ridolfi L, Albertson JD, Katul GG (2004) The effect of vegetation density on canopy sub-layer turbulence. Boundary-Layer Meteorol 111(3):565–587

Quan LH, Hu F (2009) Relationship between turbulent flux and variance in the urban canopy. Meteorol Atmosphere Phys 104(1–2):29–36

Raupach MR (1981) Conditional statistics of reynolds stress in rough-wall and smooth-wall turbulent boundary-layers. J Fluid Mech 108(Jul):363–382

Raupach MR, Thom AS (1981) Turbulence in and above plant canopies. Annu Rev Fluid Mech 13:97–129

Robinson SK (1991) Coherent motions in the turbulent boundary-layer. Annu Rev Fluid Mech 23:601–639

Rotach MW (1993a) Turbulence close to a rough urban surface.1. Reynolds stress. Boundary-Layer Meteorol 65(1–2):1–28

Rotach MW (1993b) Turbulence close to a rough urban surface.2. Variances and gradients. Boundary-Layer Meteorol 66(1–2):75–92

Roth M (1993) Turbulent transfer relationships over an urban surface.2. Integral statistics. Q J R Meteorol Soc 119(513):1105–1120

Roth M (2000) Review of atmospheric turbulence over cities. Q J R Meteorol Soc 126(564):941–990

Roth M, Oke TR (1993) Turbulent transfer relationships over an urban surface.1. spectral characteristics. Q J R Meteorol Soc 119(513):1071–1104

Roth M, Oke TR (1995) Relative efficiencies of turbulent transfer of heat, mass, and momentum over a patchy urban surface. J Atmos Sci 52(11):1863–1874

Sempreviva AM, Gryning SE (2000) Mixing height over water and its role on the correlation between temperature and humidity fluctuations in the unstable surface layer. Boundary-Layer Meteorol 97(2):273–291

Shaw RH, Tavangar J, Ward DP (1983) Structure of the reynolds stress in a canopy layer. J Clim Appl Meteorol 22(11):1922–1931

Smits AJ, McKeon BJ, Marusic I (2011) High-Reynolds number wall turbulence. Annu Rev Fluid Mech 43:353–375

Song T, Wang YS (2012) Carbon dioxide fluxes froman urban area in beijing. Atmos Res 106:139–149

Wang ZH, Bou-Zeid E, Smith JA (2013) A coupled energy transport and hydrological model for urban canopies evaluated using a wireless sensor network. Q J R Meteorol Soc 139(675):1643–1657

Warhaft Z (1976) Heat and moisture flux in the stratified boundary layer. Q J R Meteorol Soc 102(433):703–707

Webb EK, Pearman GI, Leuning R (1980) Correction of flux measurements for density effects due to heat and water vapour transfer. Q J R Meteorol Soc 106(447):85–100. doi:10.1002/qj.49710644707

Wilczak JM, Oncley SP, Stage SA (2001) Sonic anemometer tilt correction algorithms. Boundary-Layer Meteorol 99(1):127–150

Williams CA, Scanlon TM, Albertson JD (2007) Influence of surface heterogeneity on scalar dissimilarity in the roughness sublayer. Boundary-Layer Meteorol 122(1):149–165

Willmart WW, Lu 55 (1972) Structure of reynolds stress near wall. J Fluid Mech 55(Sep12):65–92

Wood CR, Lacser A, Barlow JF, Padhra A, Belcher SE, Nemitz E, Helfter C, Famulari D, Grimmond CSB (2010) Turbulent Flow at 190 m height above london during 2006–2008: a climatology and the applicability of similarity theory. Boundary-Layer Meteorol 137(1):77–96

Wu C, Murray AT (2003) Estimating impervious surface distribution by spectral mixture analysis. Remote Sens Environ 84(4):493–505. doi:10.1016/s0034-4257(02)00136-0

Wyngaard JC, Moeng CH (1992) Parameterizing turbulent-diffusion through the joint probability density. Boundary-Layer Meteorol 60(1–2):1–13

Zhao Z, Gao Z, LiD, Bi X, Liu C, Liao F (2013) Scalar flux-gradient relationships under unstable conditions over water in coastal regions. Boundary-Layer Meteorol:1–22